

Evaluation of lattice strain in ZnO thin films based on Williamson-Hall analysis

Y. MA*, Y. C. CHANG, J. Z. YIN

Jilin University, State Key Laboratory of Integrated Optoelectronics, College of Electronic Science and Engineering, Changchun 130012, China

ZnO thin films have been grown on *c*-Al₂O₃ substrates by metal-organic chemical vapor deposition at different oxygen partial pressures. The dependence of the crystallite size and the lattice strain in the ZnO thin films on the oxygen partial pressure are investigated. With increasing the oxygen partial pressure, the crystallite size is found to be reduced and the lattice strain increased by investigating Debye-Scherrer's (DS) equation and Williamson-Hall (W-H) analysis. XRD peak broadening analysis reveals that the as-grown *c*-axis oriented ZnO films are polycrystalline with the crystallite size of 23 - 43nm and the microstrain values in the range of 2.4×10^{-3} - 4.2×10^{-3} . The stress and deformation energy density calculated by W-H anisotropic models become larger as increasing the oxygen pressure. These are closely correlated to the growth mechanism of the ZnO thin films on *c*-Al₂O₃ substrates.

(Received January 7, 2019; accepted December 10, 2019)

Keywords: ZnO, MOCVD, Strain, Williamson-Hall

1. Introduction

ZnO is a promising II- VI group compound semiconductor and has attracted considerable attention for many years because of its wide direct band gap of 3.37 eV at 300K, high exciton binding energy (60 meV), as well as highly piezo electronic properties. The other advantages of ZnO include nontoxicity, high mechanical, chemical and thermal stability. These remarkable characteristics make ZnO to be an important material in optoelectronic devices, spin electronics, sensors, catalysis, solar cells, biomedicine [1-5], etc. ZnO can be grown with various nanostructure morphology, such as nanowires, nanorods, nanotubes, nano flowers, and urchin-like structures [6-11]. This distinctive morphology effect, which is attributed to the change of intrinsic defects concentration with morphology, allow us to modulate various properties and activities of nanomaterials and thus expand the applications of ZnO.

The performances of the devices depend strongly on ZnO materials quality, in which the strain is often accumulated during fabrication. Because strain is sensitive to the impurities, temperature, pressure, contact or other environmental factors compared with the bulk ZnO. For the present hetero-epitaxial ZnO thin films on *c*-sapphire, there exists large lattice mismatch (18.3%) and thermal expansion coefficient mismatch (34%) between them [12]. It is inevitable that the extrinsic strain is produced in the ZnO films, which is relaxed by forming defects. Meanwhile, the intrinsic strain originated from local heterogeneity, such as impurities or local defects, contributes to the residual strain in the films. Previous studies [13-15] have suggested that strain induced the changes of Zn-O bond length and bond angles, leading to the charge transferring and the change of electron

distribution in ZnO nanowire and bulk materials. Thus the energy shifts of the highest occupied molecular orbital (HOMO) and the lowest unoccupied molecular orbital (LUMO) occurred and the band gap changed for ZnO, even direct-to-indirect band gap transition was induced. Strain has a significant impact on the structural, morphological, electronic, optical and magnetic properties and doping efficiency of the ZnO material [16-20]. Therefore, the understanding of the strain generation and the strain induced effects is important for the manipulation of the material properties and the modulation of ZnO-based devices.

X-ray diffraction (XRD) peak profile analysis has been in general used to estimate the crystallite size and lattice strain in the materials, and other related parameters, for example, lattice stress and strain energy density can be calculated by Scherrer's equation and Williamson-Hall (W-H) analysis. Compared with other methods such as Fourier technique, Rietveld refinement and Warren-Averbach (W-A) analysis [21, 22], W-H analysis, derived from Bragg's equation, is a simplified integral breadth method that can distinguish between size related and strain related peak broadening. This is because the crystallite size depends on $1/\cos\theta$ (θ is diffraction angle), while the strain varies as $\tan\theta$. There are a number of literatures on the W-H analysis for various nanostructured materials such as AlN, ZrO₂, NiO, RuO₂, SnO₂, Y₂O₃ and ZnO [9, 23-28]. This method can interpret commendably the contributions of crystallite size and strain to the XRD peak widening through isotropic and anisotropic models. The W-H method performs well for the materials with average crystallite sizes being larger than about 10 nm [25].

In this paper, ZnO thin films are grown on *c*-sapphire (0001) substrates by metal-organic chemical vapor deposition (MOCVD) under different oxygen partial

pressures. The structure and morphology of the ZnO thin films are investigated by X-ray diffraction peak broadening analysis and Atomic force microscopy (AFM). The dependence of the crystallite size, lattice strain, stress, and deformation energy density of the ZnO thin films on the oxygen partial pressure are elucidated based on W-H analysis and Debye-Scherrer's method. Our investigation indicates the importance effect of strain on the properties of the ZnO thin films.

2. Experimental

The ZnO thin films were prepared on the c-plane sapphire substrates in MOCVD equipment. The Al_2O_3 substrates were chemically cleaned and etched in solvents for a few minutes beforehand, then thermally etched at 700°C in the reactor in situ. Diethylzinc (DEZn) and highly purified oxygen were used as Zn and O precursors, which were introduced into the chamber by individual jet nozzle. DEZn was kept at low-temperature bubbling cylinder and carried by highly purified argon into the reactor. High pure N_2 gas was introduced from the top of the reactor to prevent source gases flowing up away from the substrate. The schematic diagram of the preparation procedures for the ZnO thin films is illustrated in Fig. 1. The ZnO thin films were deposited at 470°C under different oxygen partial pressures ranging from 25, 45, 65 to 73 Pa, which corresponded to the samples a, b, c and d, respectively. The flow rate of DEZn was 9.45×10^{-5} mol/min. The substrates on the salver could rotate at a high speed of 650 rpm. The total pressure of the reactor was maintained at a constant of 260 Pa. The detailed growth conditions are listed in Table 1.

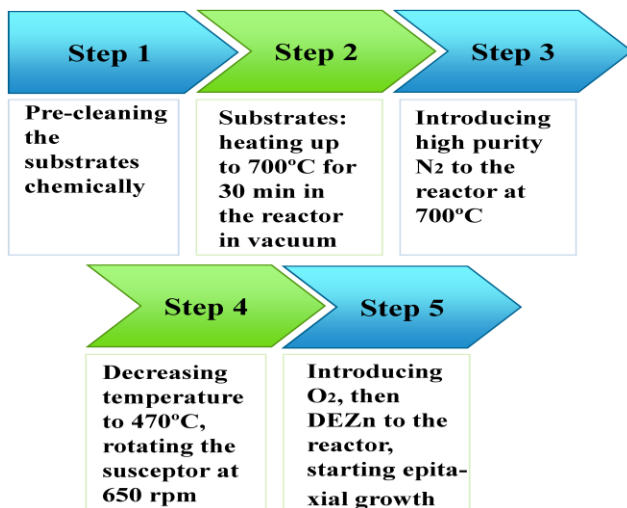


Fig. 1. Schematic diagram of the experimental procedures for the ZnO thin films grown by MOCVD

The structure and crystallinity of the ZnO films were investigated by a Rigaku wide-angle X-ray diffractometer with Cu $K\alpha$ radiation at $\lambda = 0.154$ nm. The surface morphology of the ZnO thin films prepared under different

oxygen pressures was monitored by atomic force microscope (AFM).

3. Results and discussion

The X-ray diffraction profiles of the ZnO thin films deposited at various oxygen partial pressures are shown in Fig. 2. In all the cases, the strong intensity of the (002) diffraction peak implies the preferred c-axis orientation in the hexagonal wurtzite ZnO films. During the crystal growth, the planes growing faster along the normal direction generally tend to disappear while the slower growing ones remain due to their lower surface energy. As a result, the ZnO films orient in (001) direction owing to its lowest surface energy of 1.59 J/m^2 [29].

For the samples (a) to (d) grown at different oxygen pressures, the (002) peaks are positioned at $2\theta = 34.44^\circ$, 34.52° , 34.76° and 34.76° , which shift slightly towards higher angle side compared with the unstrained bulk ZnO (34.42°), implying that a compressive strain along c-axis direction exists in the ZnO films [30]. Therefore, the films are under biaxial tensile strain paralleled to the film surface because of the Poisson effect. The intensity of (002) peaks decreases with increasing the oxygen partial pressure. Simultaneously, some weak peaks corresponding to the diffraction of (100), (101) and (102) appear in the samples (a) and (b) as shown in figure 2, and (102) diffraction peak disappear in the samples (c) and (d) with decreasing the peak intensity.

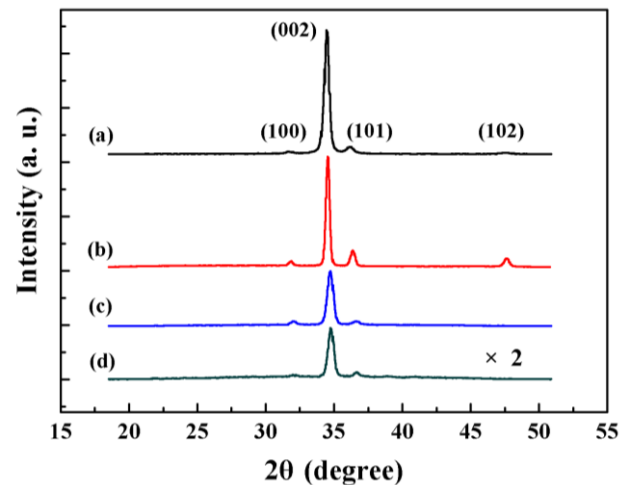


Fig. 2. X-ray diffraction patterns of the ZnO thin films grown at various oxygen partial pressures: (a) 25 Pa, (b) 45 Pa, (c) 65 Pa, (d) 73 Pa. The peak intensity of sample d is enlarged two times

As we know, vapor-phase depositions are conducted in the light of mass transport and surface reactions on the substrate. From the energy point of view, the adatoms tend to form three-dimensional (3D) clusters or islands on the surface of the substrate in the initial stages of the epitaxial growth, commonly called Volmer-Weber growth mode, when the lattice mismatch between the epilayer and the substrate materials is large [31]. The deposited materials

are firstly formed in finite 3D islands on the substrate according to István Daruka's equilibrium phase [32] for the present ZnO/Al₂O₃ (0001) strained hetero-epitaxial systems. The stable finite islands continue to grow and the adjacent islands impinge on each other to form the ripened islands, which leads to the formation of the columnar

polycrystalline ZnO thin films. In addition, at low growth temperature of 470°C, the slow diffusing rate of the adatoms on the substrate surface may reduce the crystal quality of the films. Moreover, the incomplete decomposition of DEZn may contribute to degrading the crystalline quality of ZnO.

Table 1. Growth parameters of the ZnO thin films deposited by MOCVD

Growth temperature (°C)	Flow rate of DEZn (mol/min)	Oxygen partial pressure (Pa)	Flow rate of N ₂ (sccm)	Rotation speed (rpm)	Reactor pressure (Pa)
470	9.45×10 ⁻⁵	25 45 65 73	600	650	260

Debye-Scherrer equation is generally used to estimate average crystallite size from x-ray diffraction patterns which are broadened by the instruments, crystallite size and strain. The small contribution of instrumental broadening needs to be removed from the XRD patterns by using the standard silicon. According to Debye-Scherrer (DS) equation [10]

$$D = k\lambda/\beta\cos\theta \quad (1)$$

where D is the crystallite size, k is 0.94, the shape factor, λ is the wavelength of the radiation ($\lambda = 0.154$ nm), β is the full width at half-maximum of (hkl) XRD peak corrected by instrumental broadening and θ is diffraction angle, we can obtain the relationship as follows:

$$\cos\theta = k\lambda/D \cdot (1/\beta) \quad (2)$$

The data dots are drawn with $1/\beta$ in the x-axis against $\cos\theta$ in the y-axis for the ZnO thin films prepared at various oxygen partial pressures and shown in Fig. 3. The crystallite size D is extracted from the slope of the plot by fitting the data linearly, and tabulates in Table 2.

The microstrain induced in the ZnO thin films can be calculated from Williamson-Hall method using the uniform deformation model (UDM), uniform stress deformation model (USDM) and uniform deformation energy density model (UEDM) [10]. The UDM, USDM and UEDM equations are as follows.

$$\beta\cos\theta = k\lambda/D + 4\epsilon\sin\theta \quad (3)$$

$$\beta\cos\theta = k\lambda/D + 4\sigma\sin\theta/E_{hkl} \quad (4)$$

$$\beta\cos\theta = k\lambda/D + 4\sin\theta(2/E_{hkl})^{1/2}u^{1/2} \quad (5)$$

where ϵ is the lattice microstrain, σ is the stress ($\sigma = \epsilon E_{hkl}$), E_{hkl} is Young's modulus in the $\langle hkl \rangle$ direction and u is the energy density ($u = (\epsilon^2 E_{hkl})/2$), the other parameters are the same as mentioned above. In equation (3), the strain is assumed to be uniform in all crystal orientation, while the Young's modulus (E) is considered to be anisotropic in

equations (4) and (5). Young's modulus values for the (100), (002), (101) and (102) lattice planes of the ZnO films are calculated from reference 10 to be 127.2588GPa, 144.0922GPa, 118.8582GPa and 118.3897GPa, respectively and are used in the W-H analysis.

The plots are drawn by taking ($\beta\cos\theta$) in the y-axis, $4\sin\theta$, $(4\sin\theta/E_{hkl})$ and $4\sin\theta(2/E_{hkl})^{1/2}$ in the x-axis for the ZnO films and illustrated in figures 4, 5 and 6, respectively. The strain ϵ , the deformation stress σ and the energy density u can be estimated from the slope of the fitted straight lines. Accordingly, the y-axis intersections of the fitted lines depict the crystallite size of the ZnO thin films in UDM, USDM and UEDM models. The calculations are concluded in Table 2. In the $\langle 002 \rangle$ direction, the deformation stress in the ZnO films is larger than that in the other three directions while the strain is smaller due to the assumption of the uniform deformation energy density.

For all the ZnO films, the slopes and y-intercepts of the W-H fitting lines are positive, which is meaningful physically [25]. The strain and the crystallite size calculated from the three models are in accordance with each other. The crystallite size calculated using DS method shows a little difference from that obtained by W-H models because the DS model does not consider the influence of strain on the diffraction peaks and therefore gives the smaller size.

It is observed from Table 2 that the crystallite size of the ZnO thin films decreases with increasing the oxygen partial pressure. At the lower growth temperatures, the rate of the heterogeneous nucleation occurred at the substrate surface is higher in the early growing moment and the driving force for the ZnO crystallization is larger [33]. As a result, a lot of crystal nuclei emerge at the substrate surface, which leads to small columnar grain size in the deposited ZnO thin films. The calculations using DS method and W-H analysis indicate that the average crystallite size is just about 23 - 43 nm. In the O-rich conditions, the O atoms tend to occupy the interstitial lattice site. With increasing the oxygen partial pressure, the concentration of the interstitial oxygen O_i in the ZnO films increases, and at the same time, the growth rate of the crystal nuclei speeds up. Thus the crystallites of the

films are easily misoriented and facilitate the higher density of defects, which degrades the crystal quality and forms the polycrystalline ZnO films. Accordingly, the microstrain, deformation stress and deformation energy density in the ZnO films increase when the oxygen partial pressure is increased from 25 Pa to 73 Pa as exhibited in Table 2, which increases the grain boundary density and results in the smaller crystallite size [34]. The grain

boundaries can act as potential barriers and scattering centers. Under the oxygen excess condition, larger grain boundary area cause the increase of O adsorbed in the boundaries and then increase the intergrain potential barrier height, leading to the reduction of the carrier mobility. The intergrain barrier in polycrystalline ZnO films also decreases the effective band gap.

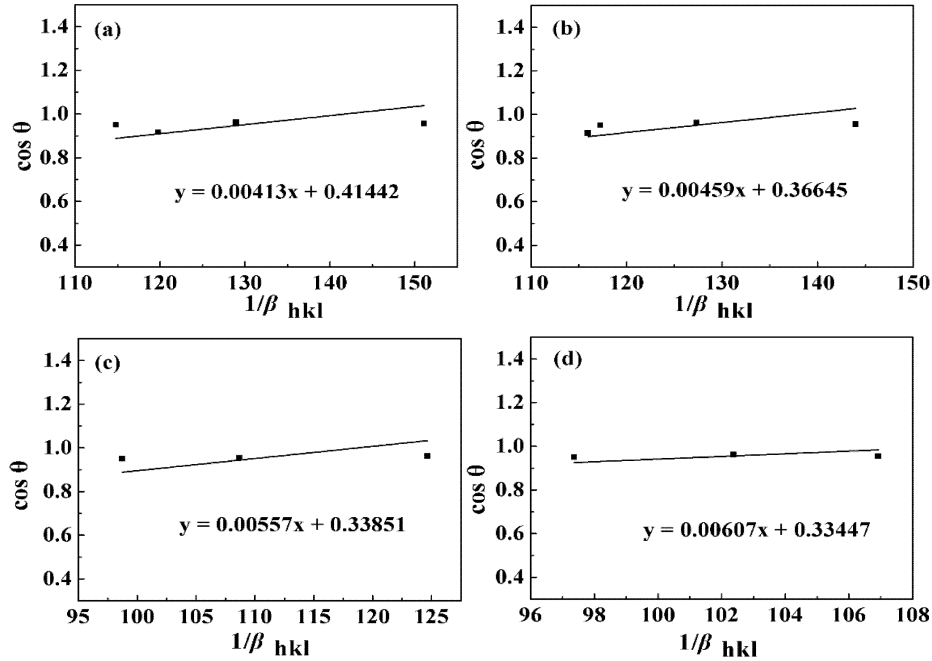


Fig. 3. Scherrer plot of $1/\beta$ vs. $\cos\theta$ of the ZnO thin films grown at various oxygen partial pressures with a linear fitting to data: (a) 25 Pa, (b) 45 Pa, (c) 65 Pa, (d) 73 Pa

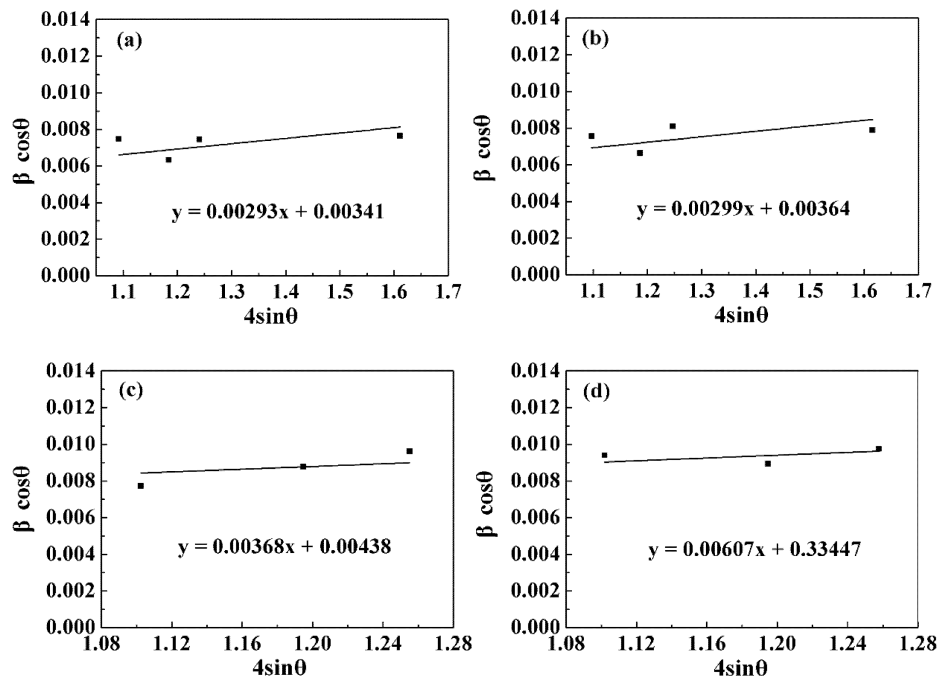


Fig. 4. The W-H analysis plot of $4\sin\theta$ vs. $\beta\cos\theta$ assuming UDM for the ZnO thin films grown at various oxygen partial pressures with a linear fitting to data: (a) 25 Pa, (b) 45 Pa, (c) 65 Pa, (d) 73 Pa

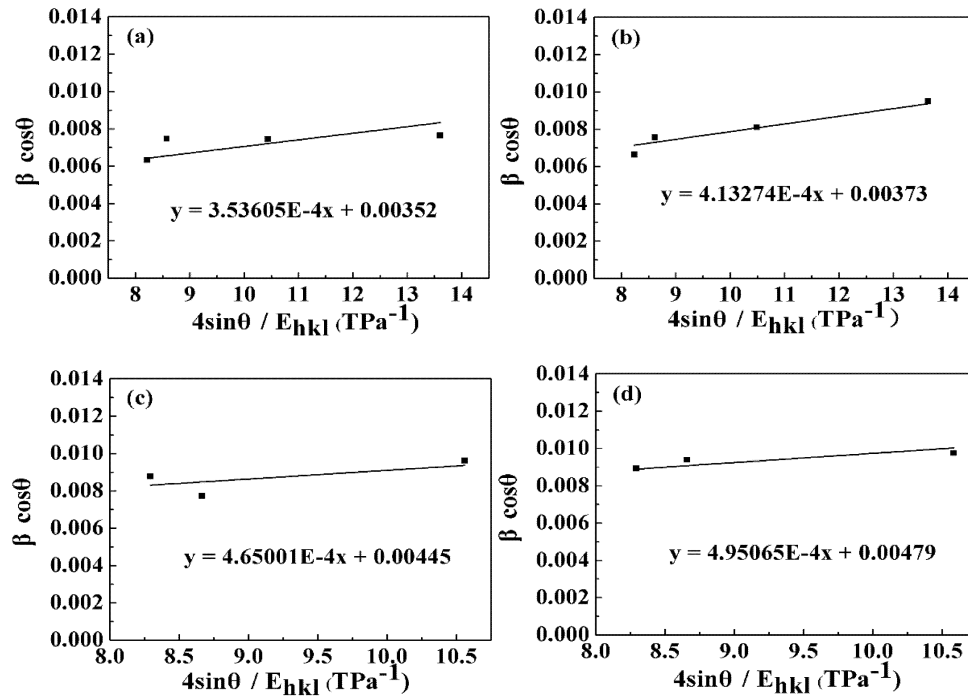


Fig. 5. The W-H analysis plot of $4\sin\theta/E_{hkl}$ vs. $\beta\cos\theta$ assuming USDM for the ZnO thin films grown at various oxygen partial pressures with a linear fitting to data: (a) 25 Pa, (b) 45 Pa, (c) 65 Pa, (d) 73 Pa

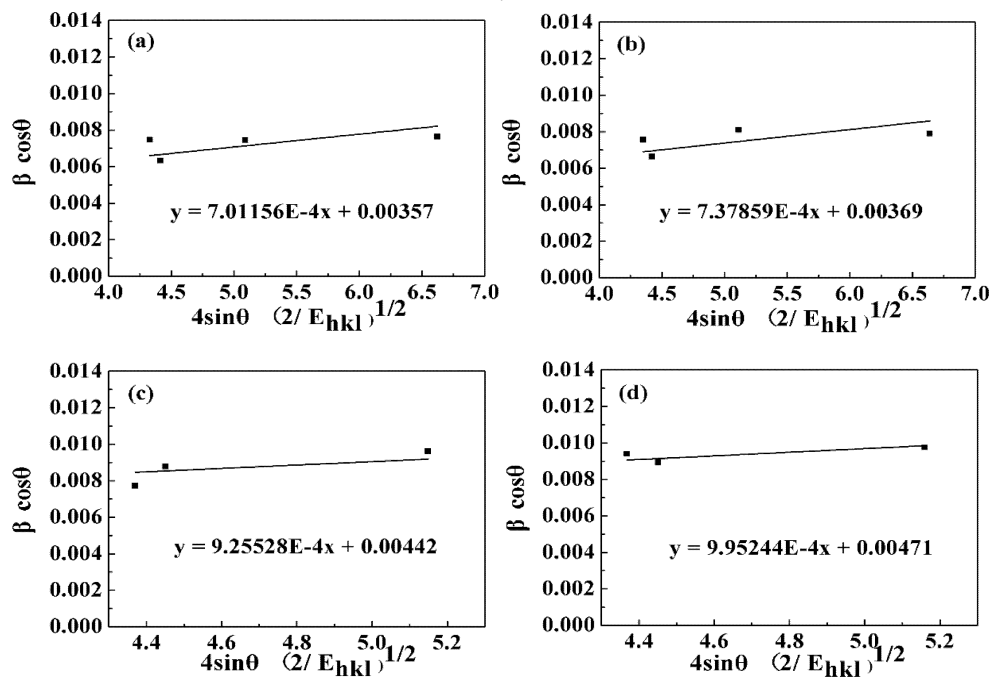


Fig. 6. The W-H analysis plot of $4\sin\theta / (2/E_{hkl})^{1/2}$ vs. $\beta\cos\theta$ assuming UDEDM for the ZnO thin films grown at various oxygen partial pressures with a linear fitting to data: (a) 25 Pa, (b) 45 Pa, (c) 65 Pa, (d) 73 Pa

Table 2. Physical parameters including crystallite size, strain, stress and energy density values calculated using DS method and W-H analysis with UDM, USDM and UDEDM models for the ZnO thin films grown at various oxygen partial pressures: (a) 25 Pa, (b) 45 Pa, (c) 65 Pa, (d) 73 Pa

sample	DS	Williamson-Hall analysis								
		UDM			USDM			UDEDM		
	D (nm)	D (nm)	ϵ (10^{-3})	D (nm)	ϵ (10^{-3})*	σ (MPa)	D (nm)	ϵ (10^{-3})*	σ (MPa)*	u (KJm^{-3})
a	35.05	42.45	2.93	41.13	2.78 ₍₁₀₀₎	353.61	40.55	2.78 ₍₁₀₀₎	353.73 ₍₁₀₀₎	491.62
					2.45 ₍₀₀₂₎			2.61 ₍₀₀₂₎	376.40 ₍₀₀₂₎	
					2.98 ₍₁₀₁₎			2.876 ₍₁₀₁₎	341.86 ₍₁₀₁₎	
					2.99 ₍₁₀₂₎			2.882 ₍₁₀₂₎	341.18 ₍₁₀₂₎	
b	31.52	39.77	2.99	38.81	3.26 ₍₁₀₀₎	413.27	39.23	2.92 ₍₁₀₀₎	372.25 ₍₁₀₀₎	544.44
					2.88 ₍₀₀₂₎			2.75 ₍₀₀₂₎	396.10 ₍₀₀₂₎	
					3.49 ₍₁₀₁₎			3.027 ₍₁₀₁₎	359.75 ₍₁₀₁₎	
					3.51 ₍₁₀₂₎			3.033 ₍₁₀₂₎	359.04 ₍₁₀₂₎	
c	25.99	33.05	3.68	32.53	3.65 ₍₁₀₀₎	465.00	32.75	3.67 ₍₁₀₀₎	466.93 ₍₁₀₀₎	856.60
					3.23 ₍₀₀₂₎			3.45 ₍₀₀₂₎	496.85 ₍₀₀₂₎	
					3.91 ₍₁₀₁₎			3.80 ₍₁₀₁₎	451.25 ₍₁₀₁₎	
					3.89 ₍₁₀₀₎			3.95 ₍₁₀₀₎	502.10 ₍₁₀₀₎	
d	23.85	29.97	3.81	30.22	3.44 ₍₀₀₂₎	495.07	30.73	3.71 ₍₀₀₂₎	534.28 ₍₀₀₂₎	990.51
					4.17 ₍₁₀₁₎			4.08 ₍₁₀₁₎	485.24 ₍₁₀₁₎	

*The subscripts of (100), (002), (101) and (102) represent the lattice planes corresponding to the anisotropic strain and stress in USDM and UDEDM models.

The strain in the films hampers coherent growth and facilitates island formation of the ZnO thin films. Strain effects can also change the ionicity and strength of the Zn-O bonds [35]. When the oxygen partial pressure is increased, the bond bending is enhanced due to the increase in the strain; hence the thermal stability of the ZnO thin films is decreased due to the increase of the strain energy density. These crystallite size and strain values obtained in the present work is similar to the previous Williamson-Hall results reported for the ZnO nanomaterials with various morphologies [6-10]. In addition, the trend that strain is increased with the decrease in the crystallite size of ZnO films is consistent with these researches. Some Williamson-Hall calculations reported in the literatures are listed in Table 3 for comparison.

It is also found that the strain in all the ZnO thin films illustrated in Table 2 is relatively small though the mismatch between the ZnO films and Al_2O_3 substrates is larger than 18%. The ZnO films with a large misfit can

grow epitaxially by domain matching epitaxy (DME), where integer multiple of lattice constants fits across ZnO/ Al_2O_3 interface [36]. Consequently, most of strain is released as a result of the formation of the misfit dislocations within certain thickness epilayers and the misfit strain could be restricted near the interface.

AFM measurements have been carried out on all the ZnO thin films grown on various oxygen pressures. Figure 7 represents the two-dimensional (2D) surface morphology of the ZnO films over a range of $2\mu\text{m}\times 2\mu\text{m}$, showing that the grain size is reduced with increasing the oxygen partial pressure, which is in accordance with the XRD results discussed above. The grain size evaluated from AFM is a bit larger than that calculated using DS method and W-H analysis. It is attributed to the presence of polycrystalline aggregates. AFM only gives the surface morphology of amalgamated grains and the crystallite size, which is the size of coherently diffracting area, is not equivalent to the grain size.

Table 3. Williamson-Hall results for ZnO nanomaterials reported in literatures

samples	technique	Williamson-Hall analysis (only showing UDM results)		References
		D (nm)	ϵ (10^{-3})	
In-doped ZnO thin film	Spray pyrolysis	61.90	2.13	6
ZnO nanopowders	Precipitation	23.224	2.369	7
ZnO nano flowers	Wet chemical method	18.0	3.118	8
ZnO nanorods	Hydrothermal method	48.31	1.05	9
ZnO nanoparticles	Sol-gel combustion method	16.19	1.2006	10

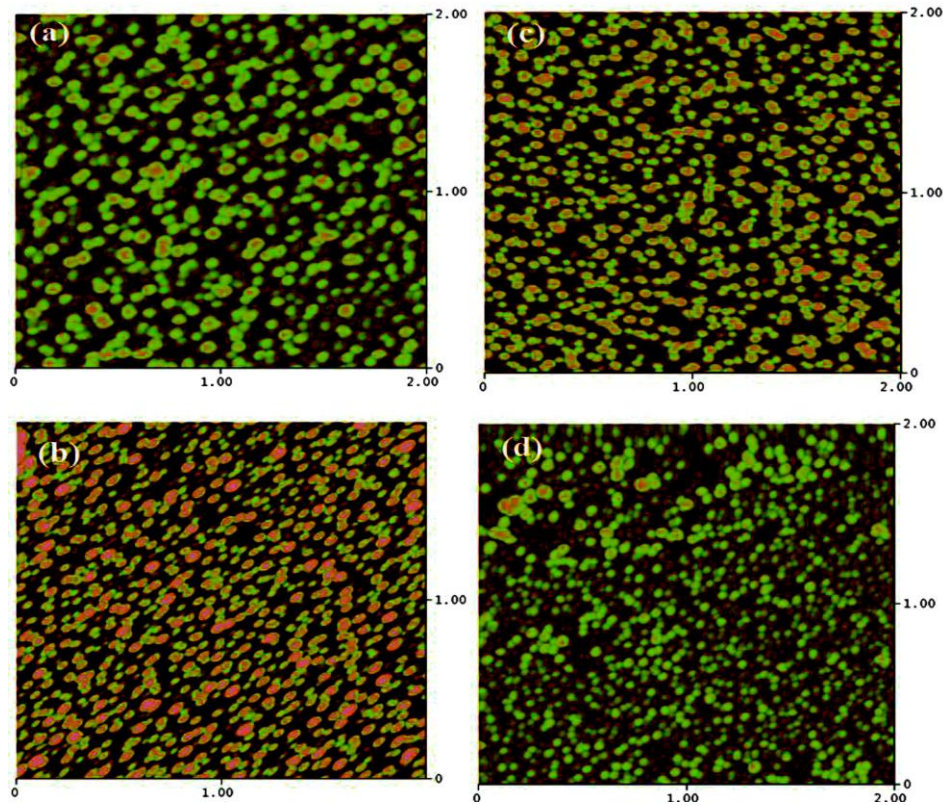


Fig. 7. AFM 2D images of the ZnO thin films grown at various oxygen partial pressures: (a) 25 Pa, (b) 45 Pa, (c) 65 Pa, (d) 73 Pa

4. Conclusions

ZnO thin films were fabricated on (0001) Al_2O_3 substrates by MOCVD under different oxygen partial pressures. It is found that the oxygen pressure influences strongly on the structure and morphology of the ZnO films. With increasing the oxygen partial pressure from 25 Pa to 73 Pa, the columnar polycrystalline ZnO films decrease in quality, subjecting to the larger compressive strain along c-axis and biaxial tensile strain parallel to the film surface. DS method and W-H analysis with isotropic and anisotropic models have revealed that the crystallite size becomes smaller and the lattice strain, deformation stress and deformation energy density increase with increase in the oxygen pressure. Larger microstrain in the ZnO thin films with 3D island growth mode decreases the crystallite size, strengthens the bond bending, and thus has a strong effect on the properties of the films.

Acknowledgments

This work was supported by the National Key Research and Development Program of China (2017YFF0105303) and National Natural Science Foundation of China (number 60877020).

References

- [1] A. Umar, A. A. Ibrahim, *J. Nanosci. Nanotechnol.* **18**(5), 3697 (2018).
- [2] C. H. Lin, S. J. Chang, T. J. Hsueh, *J. Nanosci. Nanotechnol.* **18**(2), 1202 (2018).
- [3] P. Sharma, Aaryashree, V. Garg, S. Mukherjee, *J. Appl. Phys.* **121**(22), 225306 (2017).
- [4] L. Zhu, Y. Zhang, P. Lin, Y. Wang, L. J. Yang, L. B. Chen, L. F. Wang, B. D. Chen, Z. L. Wang, *ACS Nano.* **12**(2), 1811 (2018).
- [5] S. Cheemadan, M. Krishnan, A. J. Rathinam, M. C. S. Kumar, *Mater. Res. Express* **6**(10), 104009 (2019).
- [6] H. Z. Asl, S. M. Rozati, *J. Electron. Mater.* **47**(7), 3568 (2018).
- [7] M. Kahouli, N. Tounsi, N. Mzabi, H. Guermazi, S. Guermazi, *Adv. Powder Technol.* **29**(2), 325 (2018).
- [8] E. Praveen, K. Jayakumar, *Mater. Chem. Phys.* **223**, 190 (2019).
- [9] I. J. Peter, E. Praveen, G. Vignesh, P. Nithiananthi, *Mater. Res. Express* **4**(12), 124003 (2017).
- [10] A. K. Zak, W. H. Abd. Majid, M. E. Abrishami, R. Yousefi, *Solid State Sci.* **13**(1), 251 (2011).
- [11] H. D. Kiriarachchi, K. M. Abouzeid, L. L. Bo, M. S. El-Shall, *ACS Omega* **4**(9), 14013 (2019).
- [12] S. H. Park, T. Hanada, D. C. Oh, T. Minegishi, H. Goto, G. Fujimoto, J. S. Park, I. H. Im, J. H. Chang, M. W. Cho, T. Yao, *Appl. Phys. Lett.* **91**(23), 231904 (2007).

- [13] Y. Zhang, Y. H. Wen, J. C. Zheng, Z. Z. Zhu, *Phys. Lett. A* **374**(28), 2846 (2010).
- [14] B. Wei, K. Zheng, J. Yuan, Y. Zhang, Z. Zhang, X. Han, *Nano Lett.* **12**(9), 4595 (2012).
- [15] Z. Y. Zhang, *Phys. Lett. A* **378**(16-17), 1174 (2014).
- [16] H. P. He, F. Zhuge, Z. Z. Ye, L. P. Zhu, F. Z. Wang, B. H. Zhao, J. Y. Huang, *J. Appl. Phys.* **99**(2), 023503 (2006).
- [17] Y. F. Li, B. Yao, Y. M. Lu, Y. Q. Gai, C. X. Cong, Z. Z. Zhang, X. Zhao, J. Y. Zhang, B. H. Li, D. Z. Shen, X. W. Fan, Z. K. Tang, *J. Appl. Phys.* **104**(8), 083516 (2008).
- [18] F. Schoofs, T. Fix, Ali M. H. R. Hakimi, S. S. Dhesi, G. van der Laan, S. A. Cavill, S. Langridge, J. L. MacManus-Driscoll, M. G. Blamire, *J. Appl. Phys.* **108**(5), 053911 (2010).
- [19] C. Sturm, M. Wille, J. Lenzner, S. Khujanov, M. Grundmann, *Appl. Phys. Lett.* **110**(6), 062103 (2017).
- [20] J. M. Qin, B. Yao, Y. Yan, J. Y. Zhang, X. P. Jia, Z. Z. Zhang, B. H. Li, C. X. Shan, D. Z. Shen, *Appl. Phys. Lett.* **95**(2), 022101 (2009).
- [21] S. Kundu, S. Sain, M. Yoshio, T. Kar, N. Gunawardhana, S. K. Pradhan, *Appl. Surf. Sci.* **329**, 206 (2015).
- [22] H. I. Chen, J. J. Hsiao, Y. J. Huang, J. C. Wang, Y. F. Wu, B. Y. Lu, T. E. Nee, *J. Lumin.* **168**, 304 (2015).
- [23] S. G. Pandya, J. P. Corbett, W. M. Jadwisienczak, M. E. Kordesch, *Physica E* **79**(5), 98 (2016).
- [24] K. A. Aly, N. M. Khalil, Y. Algamil, Qaid M. A. Saleem, *Mater. Chem. Phys.* **193**, 182 (2017).
- [25] K. Maniammal, G. Madhu, V. Biju, *Physica E* **85**(1), 214 (2017).
- [26] R. Sivakami, S. Dhanuskodi, R. Karvembu, *Spectrochim. Acta A* **152**, 43 (2016).
- [27] H. Köse, Ş. Karaal, Ali O. Aydin, H. Akbulut, *Mat. Sci. Semicon. Proc.* **38**, 404 (2015).
- [28] R. Srinivasan, R. Yogamalar, A. Vinu, K. Ariga, A. C. Bose, *J. Nanosci. Nanotechnol.* **9**(11), 6747 (2009).
- [29] N. Fujimura, T. Nishihara, S. Goto, J. Xu, T. Ito, *J. Cryst. Growth* **130**(1-2), 269 (1993).
- [30] Y. F. Li, B. Yao, Y. M. Lu, C. X. Cong, Z. Z. Zhang, Y. Q. Gai, C. J. Zheng, B. H. Li, Z. P. Wei, D. Z. Shen, X. W. Fan, *Appl. Phys. Lett.* **91**(7), 021915 (2007).
- [31] T. Zheleva, K. Jagannadham, J. Narayan, *J. Appl. Phys.* **75**(2), 860 (1994).
- [32] I. Daruka, A. L. Barabási, *Phys. Rev. Lett.* **79**(19), 3708 (1997).
- [33] X. F. Du, I. W. Chen, *J. Am. Ceram. Soc.* **81**(12), 3253 (1998).
- [34] R. Ghosh, D. Basak, S. Fujihara, *J. Appl. Phys.* **96**(5), 2689 (2004).
- [35] T. Kaewmaraya, A. De Sarkar, B. S. Sa, Z. Sun, R. Ahuja, *Comp. Mater. Sci.* **91**, 38 (2014).
- [36] J. Narayan, B. C. Larson, *J. Appl. Phys.* **93**(1), 278 (2003).

*Corresponding author: jlumayan@126.com